Available on the CERN CDS information server **CMS PAS SUS-16-012**

CMS Physics Analysis Summary

Contact: cms-pag-conveners-susy@cern.ch 2016/08/04

Search for Supersymmetry in Events with a Higgs Decaying to Two Photons Using the Razor Variables

The CMS Collaboration

Abstract

A search for supersymmetry is carried out in proton-proton collisions with a center of mass energy of 13 TeV and corresponding to an integrated luminosity of 15.2 fb^{-1} collected with the CMS experiment at the CERN LHC. Events are selected by requiring one Higgs boson candidate decaying into two photons in association with at least one jet. Events are categorized according to the properties of the Higgs boson candidate(s) and the razor variables (M_R and R^2) are used to improve discrimination between SUSY signals and the standard model backgrounds. The search is carried out by fitting the diphoton invariant mass distribution in each search region. The result of the search is interpreted in the context of a simplified model of bottom squark production and upper limits on the corresponding production cross section are derived.

1 Introduction

The discovery of the standard model (SM) Higgs boson at the LHC [1, 2] presents a unique opportunity to search for physics beyond the SM (BSM) using the Higgs boson as a search tool. Given the small value of the Higgs production cross section in the standard model, any BSM scenario predicting new mechanisms for Higgs boson production can be investigated with dedicated searches, using the Higgs mass to suppress SM background processes.

We present a search of this kind in pp collisions at 13 TeV using data from the CMS detector at the CERN LHC. Events with two photons consistent with a Higgs candidate are selected and categorized according to the p_T of the Higgs candidate, the presence of additional Higgs to $b\bar{b}$ or Z to $b\bar{b}$ candidates, and the estimated resolution of the diphoton pair. Motivated by supersymmetric (SUSY) scenarios, we use the razor variables [3, 4] M_R and R^2 to define search regions that may contain additional events above the SM prediction if a BSM Higgs production mechanism is present. The contribution in the search regions from the non-resonant QCD background is distinguished from a potential BSM Higgs signal using the shape of the diphoton mass distribution. The search uses 2.3 fb^{-1} of integrated luminosity collected in 2015 and 12.9 fb^{-1} collected in 2016.

In Run 1 of the LHC, a similar CMS analysis [5] reported an excess of $H \to \gamma\gamma$ events with $M_R \approx 400$ GeV and $R^2 > 0.05$ with a local (global) significance of 2.9σ (1.6σ). Motivated by the Run I result, we consider a SUSY simplified model in which bottom squarks are pair produced and decay to a bottom quark and the next-to-lightest supersymmetric particle (NLSP), $\tilde{\chi}_2^0$, with 100% branching ratio. The NLSP subsequently decays to a Higgs boson and the lightest supersymmetric particle (LSP), $\tilde{\chi}_1^0$, with 100% branching ratio. We assume that the mass difference between the NLSP and the LSP is 130 GeV, just above the Higgs boson mass. The relevant decay topology in the simplified model is shown in Figure 1. The cross section for this simplified model is assumed to be the same as the standard sbottom pair production cross section [6]. Such a signal model is observed to produce event kinematics consistent with the excess observed in Run I data and is not ruled out by searches in other final states and decay channels. This search is interpreted using the sbottom pair production model as the benchmark, and we derive limits on the production cross section as a function of the sbottom mass and the LSP mass.

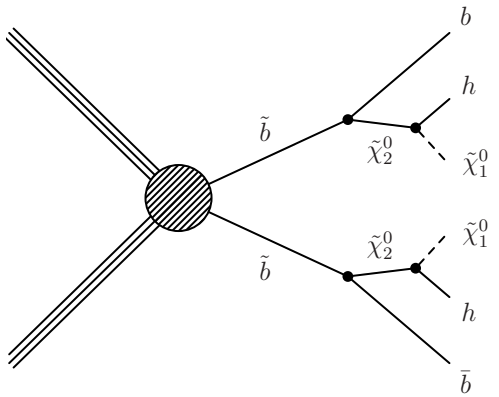

Figure 1: Diagram illustrating the SUSY benchmark simplified model of bottom squark decays to a Higgs boson, a b-jet, and the LSP.

2 Object Selection

Photon candidates with $p_T > 25$ GeV falling in the barrel region ($|\eta| < 1.4442$) are selected if they satisfy identification requirements based on the shower shape in the electromagnetic calorimeter, the hadronic to electromagnetic energy ratio, and the isolation in a cone around the photon direction [7]. To satisfy the isolation requirement, the sum of the energies of PF candidates near the photon must be smaller than a specified cut value. Isolation cuts are placed separately on energy from charged hadrons, neutral hadrons, and photons. Each isolation sum is corrected for the effect of pileup by subtracting the average energy deposited into the isolation cone estimated using a random sampling of energy density in the event. Photon objects are rejected if they match an electron candidate. The photon identification requirements correspond to a loose working point with an efficiency of about 90%.

The measured energies of the photons are corrected for clustering and local geometric effects using an energy regression trained on Monte Carlo simulation [8]. This regression gives a significant improvement to the energy resolution of the photons and provides an estimate of the uncertainty of the energy measurement. This uncertainty estimate is used in this analysis to categorize events into high and low resolution categories.

Jets are reconstructed using a global event description based on the CMS particle flow (PF) algorithm [9, 10]. Individual particles (PF candidates) are reconstructed by combining the information from the inner tracker, the calorimeters, and the muon system. Charged PF candidates associated to a vertex other than the primary one are considered pileup and are rejected. The remaining particles are clustered into jets, using the FASTJET [11] implementation of the anti-k_T [12] algorithm with the distance parameter $R = 0.4$. Jets are required not to overlap with either of the two photons; this requirement is imposed by the condition $\Delta R = \sqrt{(\Delta\eta)^2 + (\Delta\phi)^2} > 0.5$. The vector sum of the reconstructed p_T of the PF particles is used to quantify the missing transverse momentum $\vec{p}_T^{\,\text{miss}}$ in the event. Events with detector- and beam-related noise that can mimic event topologies with high energy and large $E_T^{\text{miss}} = |\vec{p}_T^{\,\text{miss}}|$ are filtered using dedicated noise reduction algorithms [13–15].

The combined secondary vertex (CSV) tagging algorithm [16] is used to identify jets originating from the showering and hadronization of b quarks. A loose working point is used which yields a mistag rate that is approximately 10%. Jet pairs are identified as $b\bar{b}$ candidates if the two jets satisfy the CSV requirement. Among all $b\bar{b}$ candidates in the event (if there are any), the pair with mass closest to 125 GeV (91.2 GeV) is chosen as a $H \to b\bar{b}$ ($Z \to b\bar{b}$) candidate. Events are not required to contain a $b\bar{b}$ pair; the presence or absence of a $H \to b\bar{b}$ or $Z \to b\bar{b}$ candidate with mass in the specified range is used in the event classification procedure described in Section 3.

3 Event Selection and Analysis Strategy

We select events with two photons that satisfy the identification criteria described above. If multiple photon pairs are identified, the pair with the largest scalar sum of the transverse momenta of the photons is chosen as the Higgs candidate. The Higgs candidate must additionally have leading photon p_T greater than 40 GeV, and diphoton mass between 103 GeV and 160 GeV.

In addition to the diphoton Higgs candidate, we require at least one additional jet with $p_T > 30$ GeV and $|\eta| < 3.0$. The Higgs candidate and all identified jets are clustered into hemispheres according to the Razor *megajet* algorithm[17], and the razor variables [3, 4] M_R and R^2 are

computed as follows:

$$M_{\mathrm{R}} \equiv \sqrt{(|\vec{p}^{j_1}| + |\vec{p}^{j_2}|)^2 - (p_z^{j_1} + p_z^{j_2})^2}, \tag{1}$$

$$\mathrm{R}^2 \equiv \left(\frac{M_{\mathrm{T}}^{\mathrm{R}}}{M_{\mathrm{R}}}\right)^2, \tag{2}$$

where $\vec{p}$ is the momentum of a hemisphere and p_z is its longitudinal component, and j_1 and j_2 are used to label the two hemispheres. In the definition of R^2, the variable $M_{\mathrm{T}}^{\mathrm{R}}$ is defined as:

$$M_{\mathrm{T}}^{\mathrm{R}} \equiv \sqrt{\frac{E_{\mathrm{T}}^{\mathrm{miss}}(p_{\mathrm{T}}^{j_1} + p_{\mathrm{T}}^{j_2}) - \vec{p}_{\mathrm{T}}^{\mathrm{miss}} \cdot (\vec{p}_{\mathrm{T}}^{j_1} + \vec{p}_{\mathrm{T}}^{j_2})}{2}}. \tag{3}$$

The razor variables M_R and R^2 provide discrimination between SUSY signal models and standard model background processes. SUSY signals typically have large values of M_R and R^2, while the standard model background exhibits an exponentially falling spectrum in both variables.

The selected events are categorized into four mutually exclusive categories. An event is categorized as "HighPt" if the p_T of the selected Higgs candidate is larger than 110 GeV. Otherwise it is categorized as "H($\gamma\gamma$)-H/Z(bb)" if the event contains two b-tagged jets whose invariant mass is in the Z mass region between 76 GeV and 106 GeV, or in the Higgs mass region between 110 GeV and 140 GeV. Remaining events are categorized as "HighRes" ("LowRes") if the mass resolution estimate σ_M/M is less (greater) than 0.85%, where σ_M is computed as $1/2 \times \sqrt{(\sigma_{E,\gamma 1}/E_{\gamma 1})^2 + (\sigma_{E,\gamma 2}/E_{\gamma 2})^2}$. The "HighPt" category is intended to isolate events from SUSY signals that produce high-p_T Higgs bosons. The "H($\gamma\gamma$)-H/Z(bb)" category is motivated by the fact that many SUSY signal models predict events with two Higgs bosons or a Higgs boson and a Z boson in the final state. Finally, the "HighRes" and "LowRes" categories are intended to capture other SUSY signals, including compressed models. The categorization procedure is illustrated in Figure 2.

Each event category is divided into bins by rectangular cuts on M_R and R^2. The binning is chosen via an optimization procedure that uses the sbottom pair production simplified model discussed in Section 1 as a benchmark model to determine the best bin boundaries. The algorithm begins with a single bin covering the entire M_R-R^2 plane. A division is made in either M_R or R^2 at the value, which maximizes the expected statistical significance. This process is repeated on each newly created bin, and until convergence is achieved. Each bin returned by the algorithm is treated as a separate analysis search region. This procedure is not performed on the LowRes category; the binning in the LowRes category is instead taken to be the same as that in the HighRes category. The definition of the individual search regions is summarized in Table 1.

To illustrate how events from a typical SUSY signal might be distributed in these bins, the distribution of events in the M_R and R^2 plane for the sbottom pair production signal model discussed in Section 1 is shown in Figures 3 and 4 for the HighPt, HighRes, and LowRes categories, respectively.

4 Background Estimation

Within each search bin, we extract a potential signal by fitting to the diphoton mass spectrum. There are two types of backgrounds: a non-resonant background that is primarily due to QCD

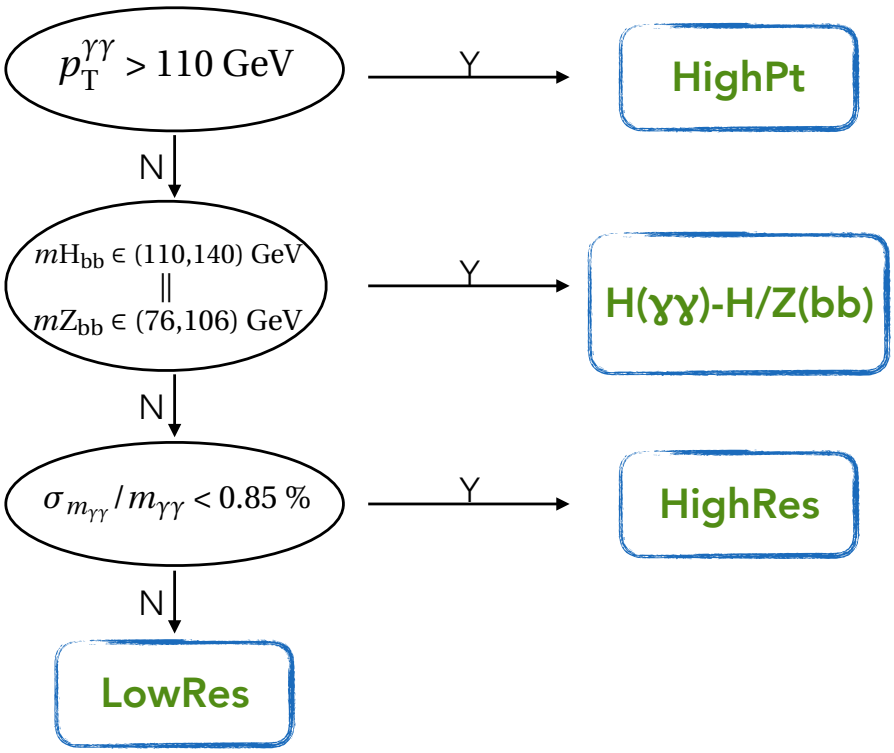

Figure 2: Diagram illustrating the event categorization used in the analysis.

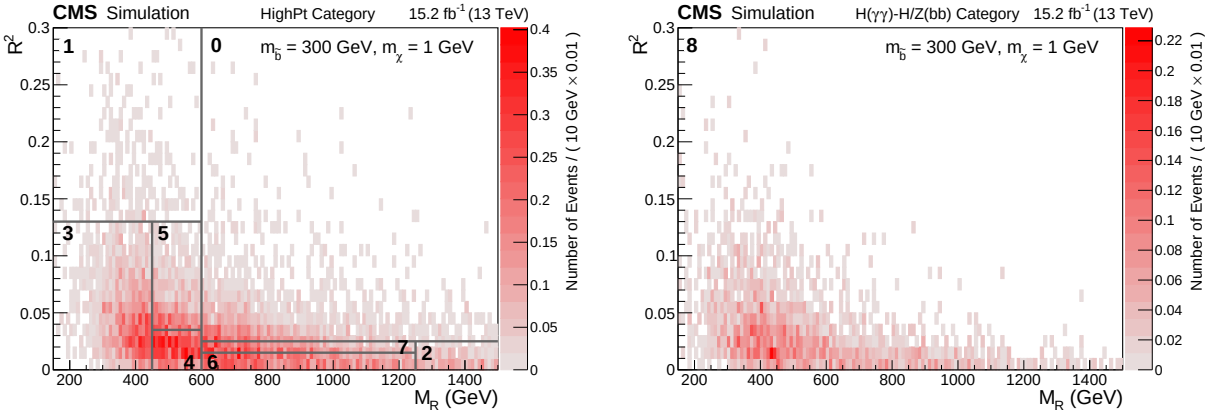

Figure 3: Distribution of events in the M_R and R^2 plane for the HighPt and H($\gamma\gamma$)-H/Z(bb) category for sbottom pair production with $m_{\tilde{b}} = 300$ GeV and $m_{\chi} = 1$ GeV. The signal expectation is shown in the color scale and the bin numbers show where each bin is located in the M_R and R^2 plane.

production of two photons or one photon and one jet, and a resonant background from standard model Higgs production. The non-resonant background is modeled with the functional form given in Table 1 for each individual search region bin, and all parameters of the function are unconstrained in the fit. The functional form model for each search region bin is selected on the basis of its Akaike Information Criterion (AIC) score [18], as well as tests of fit biases for a set of alternative models that all describe the data in the sideband well.

The standard model Higgs background and the SUSY signal are each modeled with a double-sided crystal ball function fit to the diphoton mass distribution obtained from the Monte Carlo

Table 1: A summary of the search region bins in each category is presented. The functional form used to model the non-resonant background is also listed. An exponential function of the form e^{-ax} is denoted as "singleExp"; a modified exponential function of the form e^{-ax^b} is denoted as "modExp"; and an N'th order Bernstein polynomial is denoted by "polyN".

Bin Number	Category	M_R Bin	R^2 Bin	Non-Resonant Bkg Model
0	HighPt	600 - ∞	0.025 - ∞	poly3
1	HighPt	150 - 600	0.130 - ∞	singleExp
2	HighPt	1250 - ∞	0.000 - 0.025	poly2
3	HighPt	150 - 450	0.000 - 0.130	poly2
4	HighPt	450 - 600	0.000 - 0.035	singleExp
5	HighPt	450 - 600	0.035 - 0.130	singleExp
6	HighPt	600 - 1250	0.000 - 0.015	singleExp
7	HighPt	600 - 1250	0.015 - 0.025	singleExp
8	H($\gamma\gamma$)-H/Z(bb)	150 - ∞	0.000 - ∞	singleExp
9	HighRes	150 - 250	0.000 - 0.175	modExp
10	HighRes	150 - 250	0.175 - ∞	singleExp
11	HighRes	250 - ∞	0.05 - ∞	singleExp
12	HighRes	250 - 600	0.000 - 0.05	modExp
13	HighRes	600 - ∞	0.000 - 0.05	singleExp
9	LowRes	150 - 250	0.000 - 0.175	modExp
10	LowRes	150 - 250	0.175 - ∞	singleExp
11	LowRes	250 - ∞	0.05 - ∞	modExp
12	LowRes	250 - 600	0.000 - 0.05	modExp
13	LowRes	600 - ∞	0.000 - 0.05	singleExp

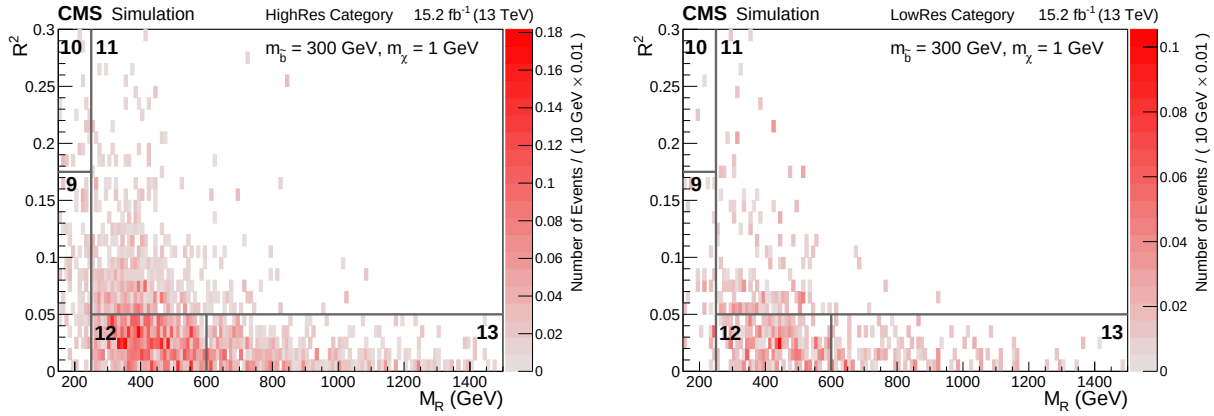

Figure 4: Distribution of events in the M_R and R^2 plane for the HighRes and LowRes categories for sbottom pair production with $m_{\tilde{b}} = 300$ GeV and $m_{\chi} = 1$ GeV. The signal expectation is shown in the color scale and the bin numbers show where each bin is located in the M_R and R^2 plane.

simulation. The parameters of each double-sided crystal ball function are held constant in the signal extraction procedure, with the exception of the parameter that determines the location of the peak. This parameter is allowed to float but is restricted via a Gaussian constraint to the region around the Higgs mass. The width of the Gaussian constraint is 1%, corresponding to the systematic uncertainty on the photon energy scale.

The normalization of the standard model Higgs background in each bin is predicted from the Monte Carlo simulation, and is constrained to that value in the fit within uncertainties. Signal yields are also predicted from the Monte Carlo simulation.

Each bin in the HighRes category is fit simultaneously with the corresponding bin in the LowRes category. The relative SM Higgs and SUSY signal yields in the two categories are constrained according to the simulation prediction. The ratio of the yields in the HighRes and LowRes categories is expected to be independent of the signal model and background process.

Nuisance parameters for various theoretical and instrumental uncertainties that can affect the SM Higgs and signal normalization and are profiled to propagate systematic uncertainties. A more detailed discussion of systematic uncertainties can be found below in Section 5. The Monte Carlo simulation predictions for the standard model Higgs background normalization are shown in Table 2 for each search region bin.

5 Systematic Uncertainties

The dominant systematic uncertainty is the uncertainty on the prediction of the non-resonant background shape and normalization. These are propagated by profiling the overall normalization and the shape parameters of the non-resonant background functional form.

Sub-dominant systematic uncertainties on the SM Higgs background are propagated through log-normal nuisance parameters, and take into account both theoretical and instrumental effects. The effects considered include missing higher order corrections, parton distribution functions, trigger and selection efficiencies, jet energy scale uncertainties, b-tagging efficiencies, and the uncertainty on the integrated luminosity. The typical size of these effects on the expected limit is summarized in Table 3.

The systematic uncertainty on the photon energy scale is implemented as a nuisance parameter that shifts the Higgs peak position, and is Gaussian constrained in the fit to lie within 1% of the nominal Higgs mass peak predicted by the Monte Carlo simulation. There is also a systematic uncertainty on the shape of the $\sigma_{\mathrm{M}}/\mathrm{M}$ distribution, which allows for migration of SM Higgs background and signal events between the HighRes and the LowRes categories.

6 Results and Interpretations

The fit results for all search regions using the combination of the 2015 dataset (2.3 fb^{-1}) and the 2016 dataset (12.9 fb^{-1}) are shown below. Figures 5, 6, and 7 show the results for the HighPt event category. The results for the H($\gamma\gamma$)-H/Z(bb) category are shown in Figure 8. Finally, the results for the HighRes and LowRes categories are shown in Figures 9 to 13.

The data yields, expected background yields, and best fit signal yields are summarized in Table 4 for all search region bins, together with the local statistical significance of the excess for each bin. The observed signal significance is summarized in Figure 14 for all statistically independent bins. The bin with the largest significance occurs in the HighPt category with $M_R > 600$ GeV and $R^2 > 0.025$, and has a local significance of 2.5σ. Accounting for the number of search region bins, this corresponds to a global significance of 1.4σ.

We interpret these results in terms of limits on the production cross-section times branching ratio for sbottom pair production with a cascade decay to a Higgs boson, a bottom quark, and the LSP. The expected and observed limits on the sbottom pair production cross section is shown in Figure 15 as a function of the sbottom mass and the LSP mass.

Table 2: The predicted yields for the standard model Higgs background processes are shown for an integrated luminosity corresponding to 15.2 fb^{-1} for each search region considered in this analysis. The contributions from each standard model Higgs process is shown separately, and the total is shown on the rightmost column along with its full uncertainty.

		Expected SM Higgs Yield					
Bin	Category	ggH	$t\bar{t}$H	VBF H	VH	bbH	Total
0	HighPt	1.09	0.49	0.17	0.25	0.01	2.0 ± 0.4
1	HighPt	0.45	0.22	0.07	0.60	0.00	1.4 ± 0.3
2	HighPt	1.75	0.23	0.89	0.07	0.02	3.0 ± 0.6
3	HighPt	20.82	0.38	4.05	2.36	0.16	27.7 ± 8.0
4	HighPt	6.30	0.20	1.77	0.45	0.06	8.8 ± 2.5
5	HighPt	1.09	0.23	0.18	0.19	0.01	1.7 ± 0.4
6	HighPt	7.15	0.21	2.91	0.28	0.05	10.7 ± 2.7
7	HighPt	1.94	0.19	0.37	0.17	0.01	2.7 ± 0.8
8	H($\gamma\gamma$)-H/Z(bb)	0.35	0.51	0.03	0.10	0.06	1.0 ± 0.2
9	HighRes	27.57	0.10	3.49	1.97	0.43	33.5 ± 10.4
10	HighRes	0.26	0.06	0.04	0.20	0.01	0.6 ± 0.1
11	HighRes	0.94	0.33	0.21	0.19	0.05	1.7 ± 0.4
12	HighRes	16.16	0.31	3.99	0.64	0.39	21.5 ± 5.4
13	HighRes	1.83	0.23	1.25	0.10	0.09	3.5 ± 1.0
9	LowRes	9.55	0.039	1.18	0.72	0.14	11.6 ± 3.8
10	LowRes	0.12	0.02	0.01	0.07	0.00	0.2 ± 0.1
11	LowRes	0.32	0.11	0.06	0.08	0.02	0.6 ± 0.2
12	LowRes	6.02	0.11	1.46	0.24	0.12	7.9 ± 2.3
13	LowRes	0.82	0.09	0.46	0.04	0.03	1.4 ± 0.4

Table 3: Summary of systematic uncertainties and their size.

Uncertainty Source	Size
Luminosity	5.7%
PDFs and QCD Scale Variations	15-30%
Trigger and selection efficiency	3%
Jet energy scale	1-5%
Photon Energy Scale	1%
B-tagging efficiency	4%
σ_M/M categorization	4%

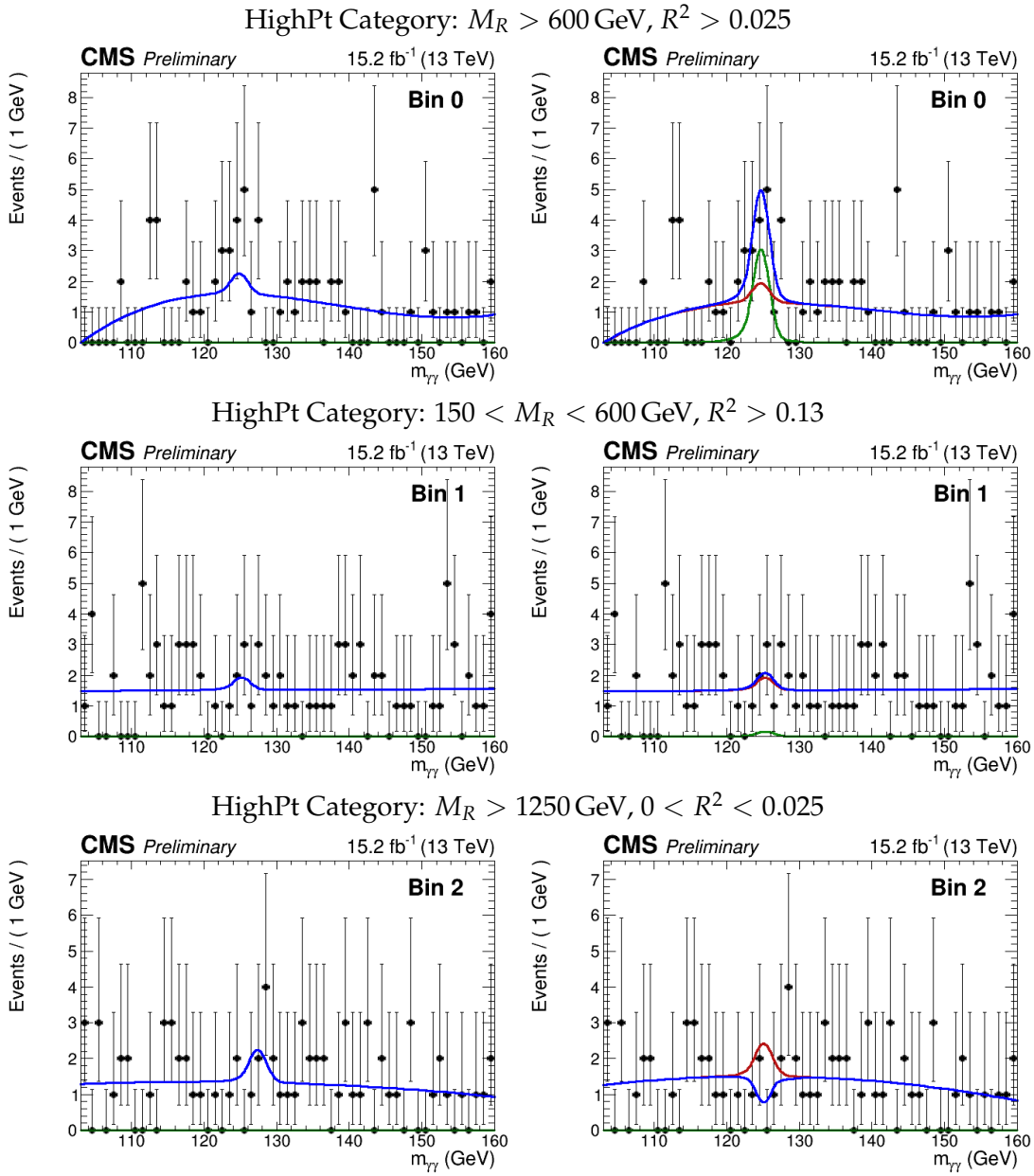

Figure 5: The diphoton mass distribution for various search region bins in the HighPt category are shown along with the background-only fit (left) and the signal plus background fit (right). The red curve represents the background prediction; the green curve represents the signal; and the blue curve represents the sum of the signal and background. The definition of the search bin is labeled above each pair of plots.

7 Summary

A search for anomalous Higgs boson production through decays of supersymmetric particles is performed with data collected in 2015 and 2016 by the CMS experiment at the CERN LHC. Proton collisions collected at a center-of-mass energy $\sqrt{s} = 13$ TeV are considered, corresponding to an integrated luminosity of about 15.2 fb^{-1} (2.3 fb^{-1} from 2015 and 12.9 fb^{-1} from 2016). Higgs boson candidates are reconstructed from pairs of photons in the central part of the detector. The razor variables M_R and R^2 are used to suppress SM Higgs boson production and other SM processes. The non-resonant background is estimated through a data-driven fit to the

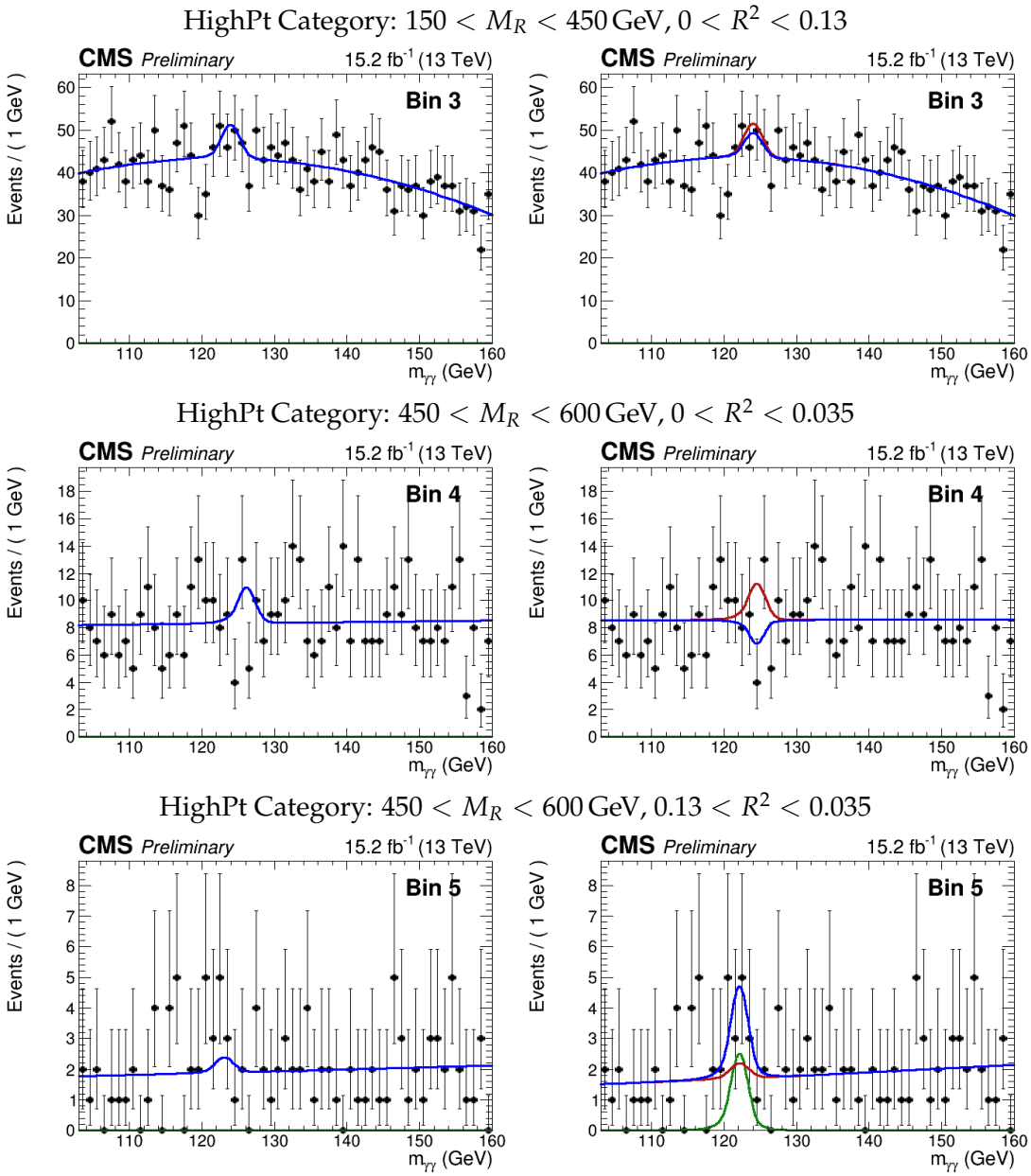

Figure 6: The diphoton mass distribution for various search region bins in the HighPt category are shown along with the background-only fit (left) and the signal plus background fit (right). The red curve represents the background prediction; the green curve represents the signal; and the blue curve represents the sum of the signal and background. The definition of the bin is labeled above each pair of plots.

diphoton mass distribution using a functional form model selected by a combination of the AIC score and the result of a series of bias tests. The standard model Higgs background is estimated using the Monte Carlo simulation, with systematics on instrumental and theoretical uncertainties propagated. We interpret the results in terms of production cross-section limits on sbottom pair production each decaying to a Higgs boson, a b-quark, and the LSP, and exclude sbottoms with mass below 350 GeV.

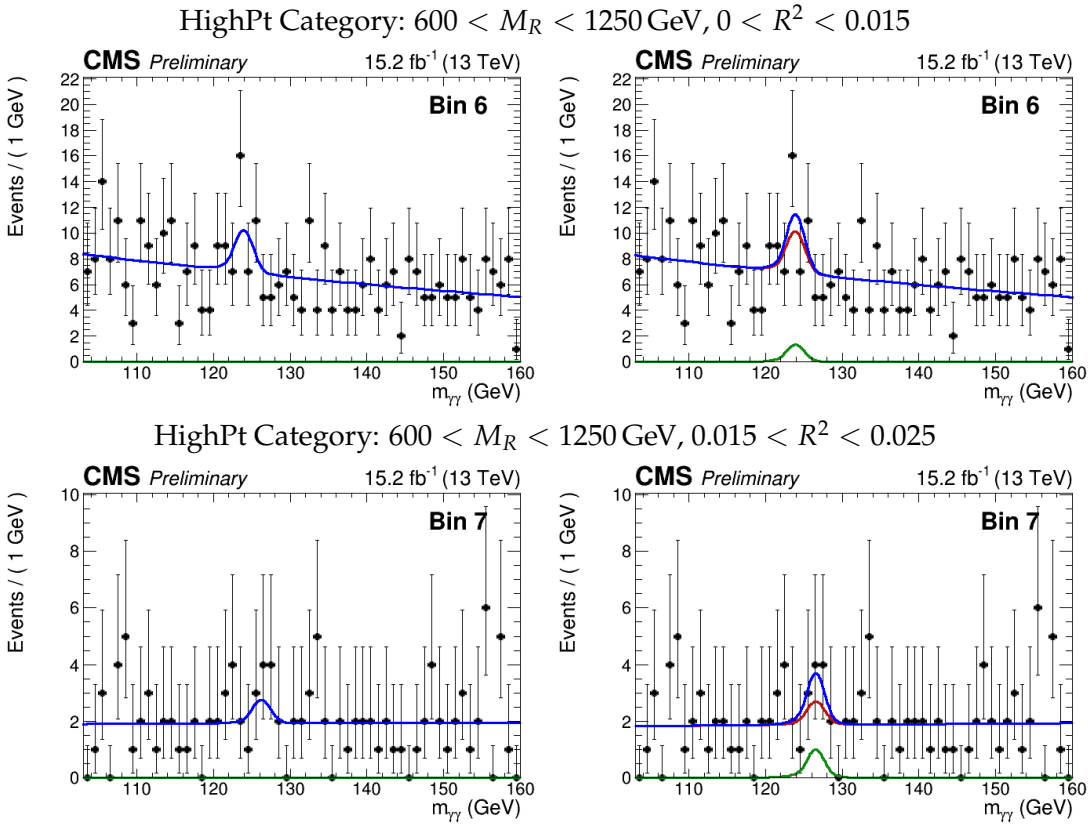

Figure 7: The diphoton mass distribution for various search region bins in the HighPt category are shown along with the background-only fit (left) and the signal plus background fit (right). The red curve represents the background prediction; the green curve represents the signal; and the blue curve represents the sum of the signal and background. The definition of the bin is labeled above each pair of plots.

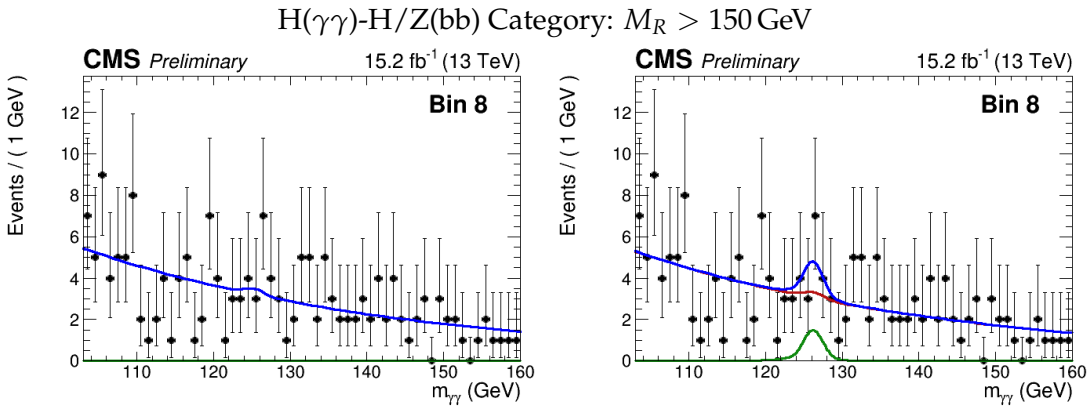

Figure 8: The diphoton mass distribution for various search region bins in the H($\gamma\gamma$)-H/Z(bb) category are shown along with the background-only fit (left) and the signal plus background fit (right). The red curve represents the background prediction; the green curve represents the signal; and the blue curve represents the sum of the signal and background. The definition of the bin is labeled above each pair of plots.

References

[1] ATLAS Collaboration, "Observation of a new particle in the search for the Standard

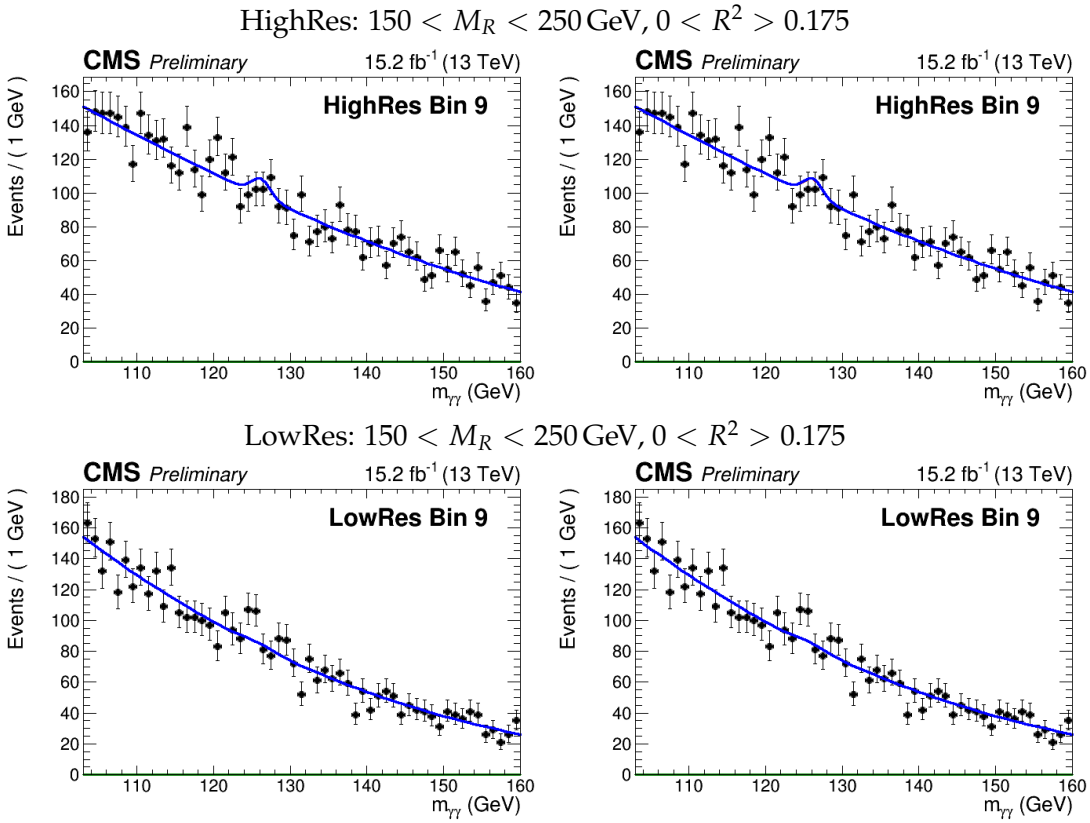

Figure 9: The diphoton mass distribution for the search region bin 9 are shown along with the background-only fit (left) and the signal plus background fit (right). The top row shows the HighRes category, while the bottom row shows the LowRes category. The red curve represents the background prediction; the green curve represents the signal; and the blue curve represents the sum of the signal and background. The definition of the bin is labeled above each pair of plots.

Model Higgs boson with the ATLAS detector at the LHC", *Phys. Lett. B* **716** (2012) 1, doi:10.1016/j.physletb.2012.08.020, arXiv:1207.7214.

[2] CMS Collaboration, "Observation of a new boson at a mass of 125 GeV with the CMS experiment at the LHC", *Phys. Lett. B* **716** (2012) 30, doi:10.1016/j.physletb.2012.08.021, arXiv:1207.7235.

[3] CMS Collaboration, "Inclusive search for squarks and gluinos in pp collisions at $\sqrt{s} = 7$ TeV", *Phys. Rev. D* **85** (2012) 012004, doi:10.1103/PhysRevD.85.012004, arXiv:1107.1279.

[4] C. Rogan, "Kinematics for new dynamics at the LHC", (2010). arXiv:1006.2727.

[5] CMS Collaboration, "Search for SUSY with Higgs in the diphoton final state using the razor variables", CMS Physics Analysis Summary CMS-PAS-SUS-14-017, 2014.

[6] C. Borschensky et al., "Squark and gluino production cross sections in pp collisions at $\sqrt{s}$ = 13, 14, 33 and 100 TeV", *Eur. Phys. J.* **C74** (2014), no. 12, 3174, doi:10.1140/epjc/s10052-014-3174-y, arXiv:1407.5066.

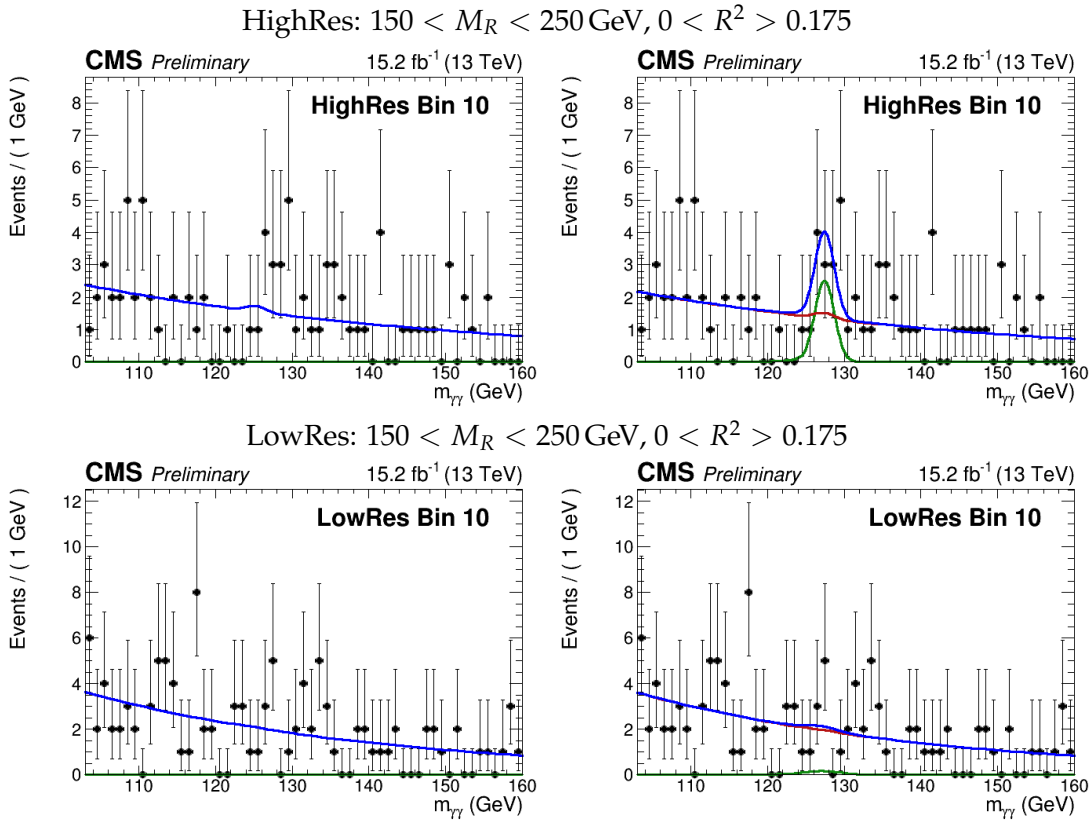

Figure 10: The diphoton mass distribution for the search region bin 10 are shown along with the background-only fit (left) and the signal plus background fit (right). The top row shows the HighRes category, while the bottom row shows the LowRes category. The red curve represents the background prediction; the green curve represents the signal; and the blue curve represents the sum of the signal and background. The definition of the bin is labeled above each pair of plots.

[7] CMS Collaboration, "Observation of the diphoton decay of the Higgs boson and measurement of its properties", *Eur. Phys. J. C* **74** (2014) 3076, doi:10.1140/epjc/s10052-014-3076-z, arXiv:1407.0558.

[8] CMS Collaboration, "Performance of Photon Reconstruction and Identification with the CMS Detector in Proton-Proton Collisions at sqrt(s) = 8 TeV", *JINST* **10** (2015), no. 08, P08010, doi:10.1088/1748-0221/10/08/P08010, arXiv:1502.02702.

[9] CMS Collaboration, "Particle–flow event reconstruction in CMS and performance for jets, taus, and $E_{\mathrm{T}}^{\mathrm{miss}}$", CMS Physics Analysis Summary CMS-PAS-PFT-09-001, 2009.

[10] CMS Collaboration, "Commissioning of the particle-flow event reconstruction with the first LHC collisions recorded in the CMS detector", CMS Physics Analysis Summary CMS-PAS-PFT-10-011, 2010.

[11] M. Cacciari, G. P. Salam, and G. Soyez, "FastJet user manual", *Eur. Phys. J. C* **72** (2012) 1896, doi:10.1140/epjc/s10052-012-1896-2, arXiv:1111.6097.

[12] M. Cacciari, G. P. Salam, and G. Soyez, "The anti-k_{T} jet clustering algorithm", *JHEP* **04** (2008) 063, doi:10.1088/1126-6708/2008/04/063, arXiv:0802.1189.

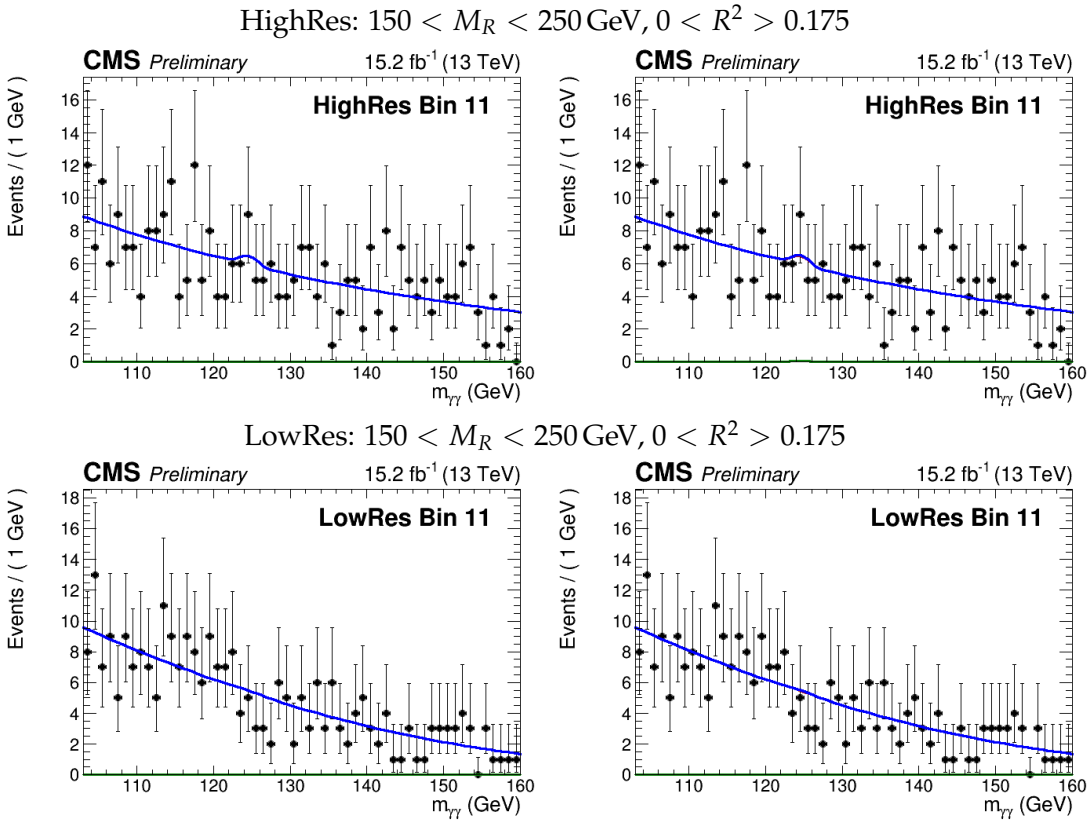

Figure 11: The diphoton mass distribution for the search region bin 11 are shown along with the background-only fit (left) and the signal plus background fit (right). The top row shows the HighRes category, while the bottom row shows the LowRes category. The red curve represents the background prediction; the green curve represents the signal; and the blue curve represents the sum of the signal and background. The definition of the bin is labeled above each pair of plots.

[13] CMS Collaboration, "Missing transverse energy performance of the CMS detector", *JINST* **6** (2011) P09001, doi:10.1088/1748-0221/6/09/P09001, arXiv:1106.5048.

[14] CMS Collaboration, "Search for New Physics in the Multijet and Missing Transverse Momentum Final State in Proton-Proton Collisions at $\sqrt{s} = 7$ TeV", *Phys. Rev. Lett.* **109** (2012) 171803, doi:10.1103/PhysRevLett.109.171803, arXiv:1207.1898.

[15] CMS Collaboration, "Performance of the missing transverse energy reconstruction by the CMS experiment in $\sqrt{s}$ = 8 TeV pp data", CMS Physics Analysis Summary CMS-PAS-JME-13-003, 2013.

[16] CMS Collaboration, "Performance of b tagging at $\sqrt{s} = 8$ TeV in multijet, $t\bar{t}$ and boosted topology events", CMS Physics Analysis Summary CMS-PAS-BTV-13-001, 2013.

[17] CMS Collaboration, "Search for supersymmetry with razor variables in pp collisions at $\sqrt{s}$ = 7 TeV", *Phys. Rev. D* **90** (2014) 112001, doi:10.1103/PhysRevD.90.112001, arXiv:1405.3961.

[18] H. Akaike, "A new look at the statistical model identification", *IEEE Transactions on Automatic Control* **19-6** (1974) 716–723, doi:10.1109/TAC.1974.1100705.

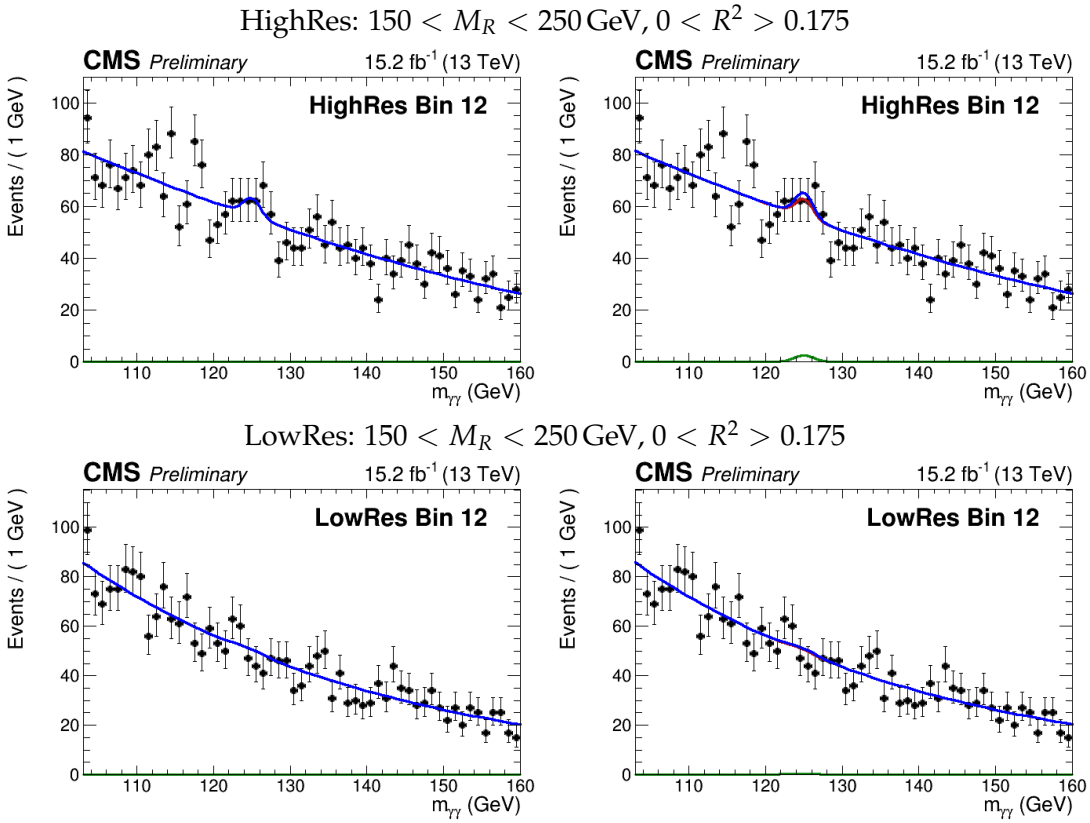

Figure 12: The diphoton mass distribution for the search region bin 12 are shown along with the background-only fit (left) and the signal plus background fit (right). The top row shows the HighRes category, while the bottom row shows the LowRes category. The red curve represents the background prediction; the green curve represents the signal; and the blue curve represents the sum of the signal and background. The definition of the bin is labeled above each pair of plots.

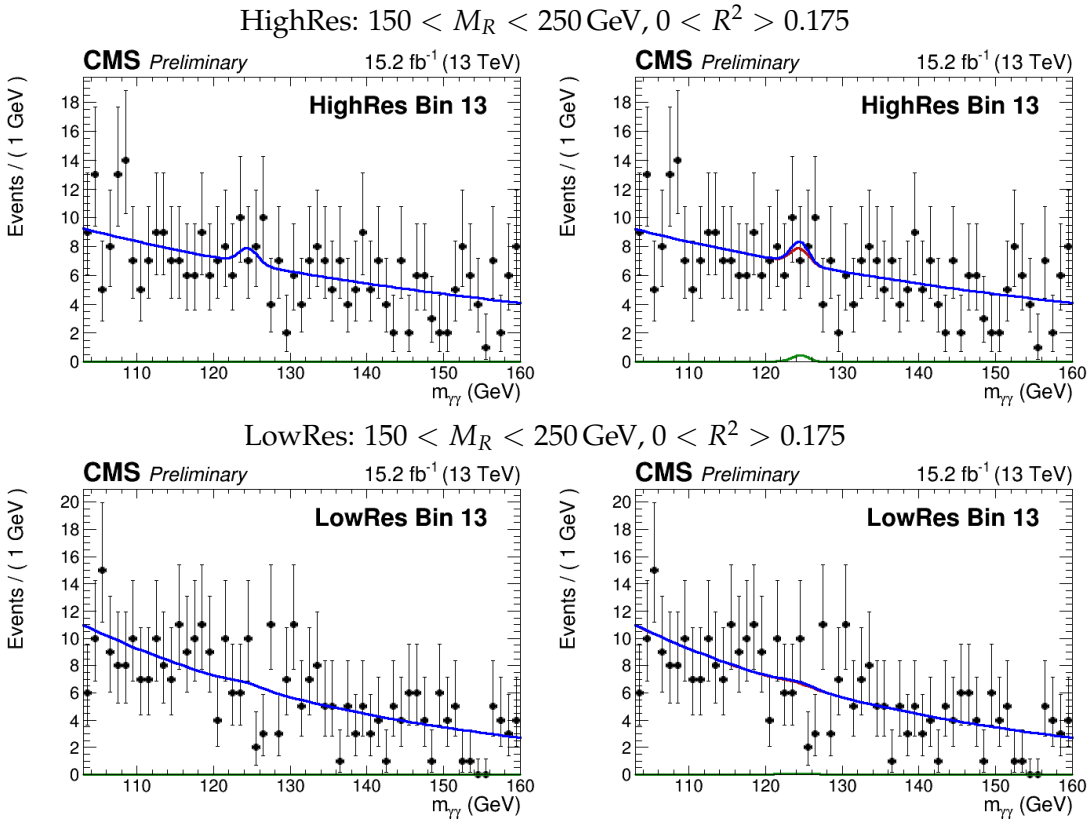

Figure 13: The diphoton mass distribution for the search region bin 13 are shown along with the background-only fit (left) and the signal plus background fit (right). The top row shows the HighRes category, while the bottom row shows the LowRes category. The red curve represents the background prediction; the green curve represents the signal; and the blue curve represents the sum of the signal and background. The definition of the bin is labeled above each pair of plots.

Table 4: The non-resonant background yields, SM Higgs background yields, best fit signal yields, and observed local significance are shown for the signal plus background fit in each search region bin. The uncertainties include both statistical and systematic components. The non-resonant background yields shown correspond to the yield within the window between 122 GeV and 129 GeV and is intended to better reflect the background under the signal peak. The observed significance for the bins in HighRes and LowRes categories are identical because they are the result of a simultaneous fit. The significance is computed using the profile likelihood, where the sign reflects whether an excess (positive sign) or deficit (negative sign) is observed.

		Yields				Obs. Local
Bin	Category	Non-Resonant Bkg	Exp. SM Higgs	Fitted SM Higgs	Best Fit Signal	Significance
0	HighPt	10.2 ± 1.4	2.0 ± 0.4	2.0 ± 0.7	9.7 ± 5.1	2.5σ
1	HighPt	10.5 ± 1.3	1.4 ± 0.3	1.4 ± 0.3	0.5 ± 3.4	0.2σ
2	HighPt	10.5 ± 1.6	3.0 ± 0.6	2.9 ± 0.9	-5.2 ± 2.5	-1.4σ
3	HighPt	304 ± 16.6	27.7 ± 8.0	27.7 ± 11.2	-7.9 ± 18.1	-0.4σ
4	HighPt	60 ± 3.0	8.8 ± 2.5	8.8 ± 3.5	-13.9 ± 6.6	-1.6σ
5	HighPt	12.1 ± 1.4	1.7 ± 0.4	1.7 ± 0.6	8.3 ± 4.7	1.9σ
6	HighPt	47.6 ± 2.6	10.7 ± 2.7	10.7 ± 3.7	4.1 ± 7.3	0.6σ
7	HighPt	13.1 ± 1.4	2.7 ± 0.8	2.7 ± 1.0	3.2 ± 4.1	0.8σ
8	H($\gamma\gamma$)-H/Z(bb)	21.6 ± 1.8	1.0 ± 0.2	1.0 ± 0.2	5.3 ± 4.6	1.0σ
9	HighRes	697 ± 10.6	33.5 ± 10.4	33.2 ± 12.1	0.0 ± 21.4	-0.2σ
10	HighRes	9.8 ± 1.2	0.6 ± 0.1	0.6 ± 0.1	8.2 ± 4.1	1.7σ
11	HighRes	40.7 ± 2.4	1.7 ± 0.4	1.7 ± 0.6	0.2 ± 5.5	0.0σ
12	HighRes	387 ± 14.6	21.5 ± 5.4	21.5 ± 9.1	8.1 ± 14.9	0.5σ
13	HighRes	46.8 ± 2.6	3.5 ± 1.0	3.5 ± 1.2	1.3 ± 6.0	0.2σ
9	LowRes	591 ± 9	11.6 ± 3.8	11.9 ± 5.1	0.2 ± 10.1	-0.2σ
10	LowRes	14.1 ± 1.4	0.2 ± 0.1	0.2 ± 0.1	1.1 ± 0.8	1.7σ
11	LowRes	36.6 ± 9.2	0.6 ± 0.3	0.6 ± 0.3	0.1 ± 1.8	0.0σ
12	LowRes	341 ± 7	7.9 ± 2.3	7.9 ± 3.5	2.8 ± 5.0	0.5σ
13	LowRes	44.3 ± 2.4	1.4 ± 0.4	1.4 ± 0.7	0.5 ± 2.6	0.2σ

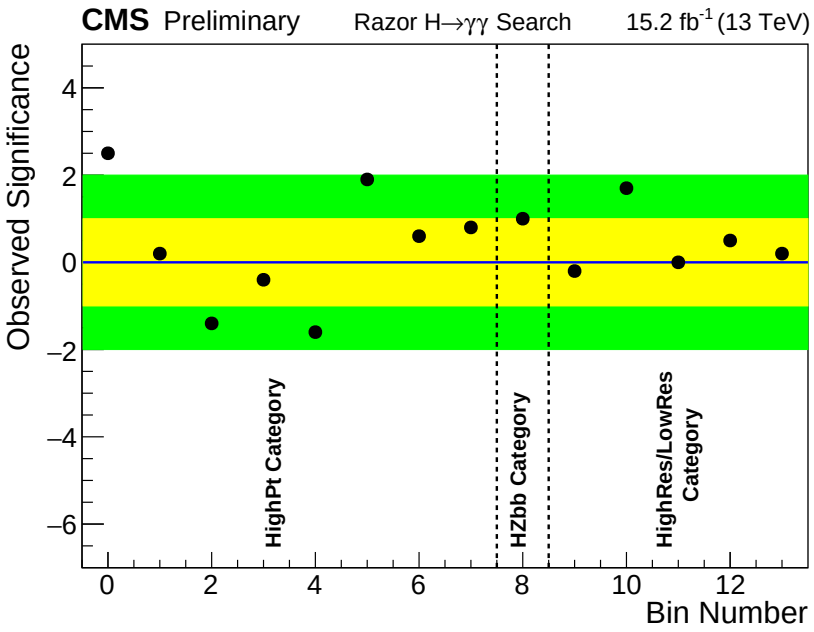

Figure 14: The observed significance in units of standard deviations is plotted for each search bin. The significance is computed using the profile likelihood, where the sign reflects whether an excess (positive sign) or deficit (negative sign) is observed. The categories that the bins belong to are labeled at the bottom. The yellow and green bands represent the 1σ and 2σ regions, respectively.

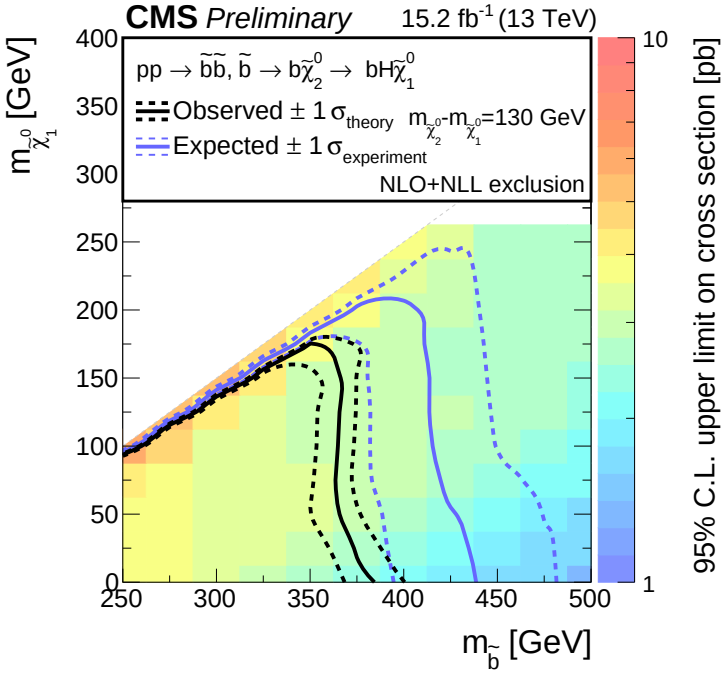

Figure 15: The observed 95% confidence level (C.L.) upper limits on the production cross section for sbottom pair production decaying to a bottom quark, a Higgs boson, and the LSP are shown. The solid and dotted black contours represent the observed exclusion region and its 1σ bands, while the analogous blue contours represent the expected exclusion region and its 1σ bands.